doi:10.1038/nature20799

Lasing action from photonic bound states in continuum

Ashok Kodigala[1]*, Thomas Lepetit[1]*, Qing Gu[1]*, Babak Bahari[1], Yeshaiahu Fainman[1] & Boubacar Kanté[1]

In 1929, only three years after the advent of quantum mechanics, von Neumann and Wigner showed that Schrödinger's equation can have bound states above the continuum threshold[1]. These peculiar states, called bound states in the continuum (BICs), manifest themselves as resonances that do not decay. For several decades afterwards the idea lay dormant, regarded primarily as a mathematical curiosity. In 1977, Herrick and Stillinger revived interest in BICs when they suggested that BICs could be observed in semiconductor superlattices[2,3]. BICs arise naturally from Feshbach's quantum mechanical theory of resonances, as explained by Friedrich and Wintgen, and are thus more physical than initially realized[4]. Recently, it was realized that BICs are intrinsically a wave phenomenon and are thus not restricted to the realm of quantum mechanics. They have since been shown to occur in many different fields of wave physics including acoustics, microwaves and nanophotonics[5–16]. However, experimental observations of BICs have been limited to passive systems and the realization of BIC lasers has remained elusive. Here we report, at room temperature, lasing action from an optically pumped BIC cavity. Our results show that the lasing wavelength of the fabricated BIC cavities, each made of an array of cylindrical nanoresonators suspended in air, scales with the radii of the nanoresonators according to the theoretical prediction for the BIC mode. Moreover, lasing action from the designed BIC cavity persists even after scaling down the array to as few as 8-by-8 nanoresonators. BIC lasers open up new avenues in the study of light–matter interaction because they are intrinsically connected to topological charges[17] and represent natural vector beam sources (that is, there are several possible beam shapes)[18], which are highly sought after in the fields of optical trapping, biological sensing and quantum information.

Cavities play a fundamental role in wave phenomena from quantum mechanics to electromagnetism and dictate the spatiotemporal physics of lasers. In general, they are constructed by closing all channels through which waves can escape. We report, at room temperature (295 K), a BIC laser that harnesses optical modes residing in the radiation continuum but, nonetheless, possess arbitrarily high quality factors, Q. These counterintuitive cavities are based on resonance-trapped, symmetry-compatible modes that destructively interfere.

Generally, open systems are described by non-Hermitian effective Hamiltonians that have multivariate and complex eigenvalues describing modes of the system. These eigenvalues exist in a multidimensional hyperspace but, in a given frequency range, the investigation can be reduced to a finite number of variables, thus limiting the complexity of the effective Hamiltonian[7]. When eigenvalues come close to crossing as a function of a geometrical parameter that modifies the system, avoided resonance crossing occurs, that is, eigenvalues repel each other in the entire complex plane[19–21]. Friedrich and Wintgen showed that resonance-trapped BICs represent a particular type of avoided resonance crossing for which coupling occurs predominantly in the far-field.

Our system consists of a thin membrane of semiconductor material suspended in air. We subsequently structure the membrane at the nanometre scale. The field in the air is a superposition of independent waves, which are interpreted as decay channels, and can be either propagating or evanescent. The field in the membrane, which becomes a superposition of coupled waves owing to structuring, is also coupled to the field in air. In the resulting open system described by a non-Hermitian Hamiltonian, the imaginary part of the complex eigenfrequency serves to quantify the decay of modes via the resonance lifetime. This lifetime is governed by coupling amongst different waves within the membrane through the Fourier coefficients of the periodic permittivity. A precise engineering of coupling among relevant waves in reciprocal space can lead to total destructive interference, that is, an infinite lifetime (see section A of Supplementary Information). BICs arise in the limit when a complex eigenfrequency mode tends towards a purely real eigenfrequency mode. They are very peculiar discrete modes in that they are actually embedded within the continuous spectrum but intrinsically possess an infinitely high radiation quality factor as a result of their

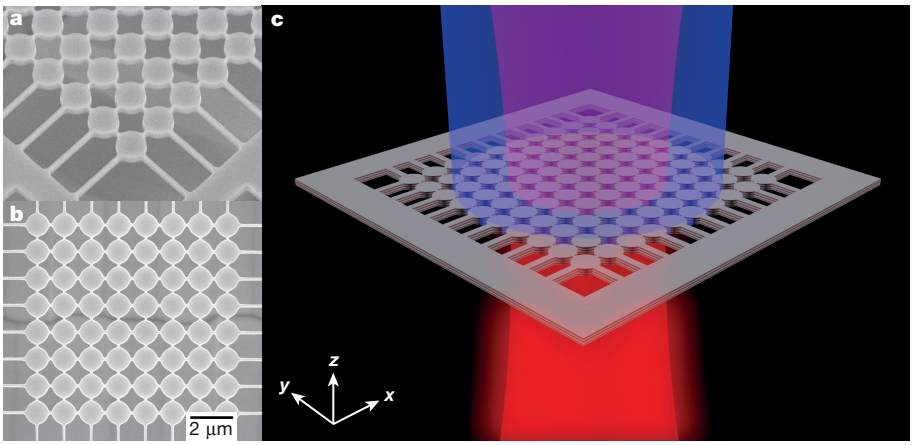

Figure 1 | BIC laser. a, Tilted electron micrograph of InGaAsP multiple quantum wells cylindrical nanoresonator array suspended in air. All structures are fabricated using electron beam lithography followed by reactive ion etching to form the cylinders. We subsequently use wet etching to suspend the structure (see section B of Supplementary Information). **b**, Top view of an 8-by-8 array with supporting bridges, which are used for the mechanical stability of the membrane. The dimensions of the structure are the period (1,200 nm), the thickness (300 nm) and the bridge width (200 nm). **c**, Schematic of the fabricated system illustrating the pump beam (blue) and lasing from the BIC mode (red). The radius of the cylindrical nanoresonators is the key parameter in our BIC design.

[1]Department of Electrical and Computer Engineering, University of California San Diego, La Jolla, California 92093-0407, USA.
*These authors contributed equally to this work.

© 2017 Macmillan Publishers Limited, part of Springer Nature. All rights reserved.

non-decaying nature. BICs are thus ideally suited for the design of perfect nanophotonic cavities.

As shown in Fig. 1, our BIC cavity is composed of a periodic array of nanoresonators of radius R interconnected by a network of supporting bridges used for the mechanical stability of the system. The membrane consists of several $In_xGa_{1-x}As_yP_{1-y}$ multiple quantum wells, specially designed to operate around the telecommunication wavelength ($\lambda \approx 1.55\,\mu m$). The radius of the cylindrical nanoresonators is the only parameter we use to tune the modes of the membrane and alter the effective Hamiltonian. The structure is fabricated using electron-beam lithography and reactive ion etching to define the cylindrical nanoresonators, followed by a wet etching step to create the membrane (see section B of Supplementary Information). It is worth noting that the radii of the fabricated nanoresonators are always smaller than their nominal design values, a consequence of reactive ion etching. As a result, the maximum achievable radius is strictly smaller than $a/2$ where a is the period of our structure.

To analyse our system, we calculate the quality factors at normal incidence around 1.55 μm, that is, within the gain bandwidth of the material. The system was modelled using a three-dimensional finite-element-method eigenfrequency solver. We restrict the discussion to odd modes (transverse-magnetic-like) as they have much higher quality factors than even modes (transverse-electric-like) in the wavelength range of interest (see section C of Supplementary Information). We find three modes around 1.55 μm with appreciable quality factors, one doubly degenerate mode (modes 1 and 2) and one singly degenerate mode (mode 3). Figure 2a shows their quality factor as a function of the radius ($522\,nm \leq R \leq 534\,nm$). The quality factor of mode 3 is independent of the radius and remains high throughout the calculated range. This mode corresponds to a symmetry-protected mode[22]. In contrast, the quality factor of modes 1 and 2 depends strongly on the radius and reaches a maximum at an optimum radius of $R_{opt} = 528.4\,nm$. At this optimum radius, modes 1 and 2 completely decouple from the radiation continuum and thus become BICs. This mode corresponds to a resonance-trapped mode (see section D of Supplementary Information).

The quality factor can diverge in two different situations. In the first situation (mode 3), coupling to the outside vanishes solely as a result of symmetry mismatch. Any perturbation that preserves symmetry, such as a modification of the radius, has no impact on its quality factor. This type of mode has been extensively studied before[23]. In the second situation (modes 1 and 2), coupling to the outside vanishes as a result of total destructive interference[13,24]. This BIC mode (resonance-trapped) is fundamentally different from previous works on band-edge lasers[25–27] (symmetry-protected) that are restricted to high symmetry points of the reciprocal lattice (see section E of Supplementary Information). Resonance-trapped BICs achieve an infinite quality factor at the singular radius R_{opt} but the quality factor remains very high for radii around R_{opt}. Figure 2b shows the transmission spectrum at normal incidence of our structure, in which the quality factor of modes 1 and 2 can be seen to tend slowly to infinity from its vanishing linewidth.

Figure 2c shows the dispersion relation of the BIC structure at $R = R_{opt}$ along the MΓ and ΓX directions. Here Γ, X, and M are high-symmetry points of the first Brillouin zone for a square lattice. We also plot the complex dispersion relation of modes 1 and 2 (Fig. 2d, e) and mode 3 (Fig. 2f). Figure 2f shows that mode 3 is extremely sensitive to symmetry-breaking perturbations as its quality factor drops sharply away from the Γ point. Quality factors of modes 1 and 2, which are no longer

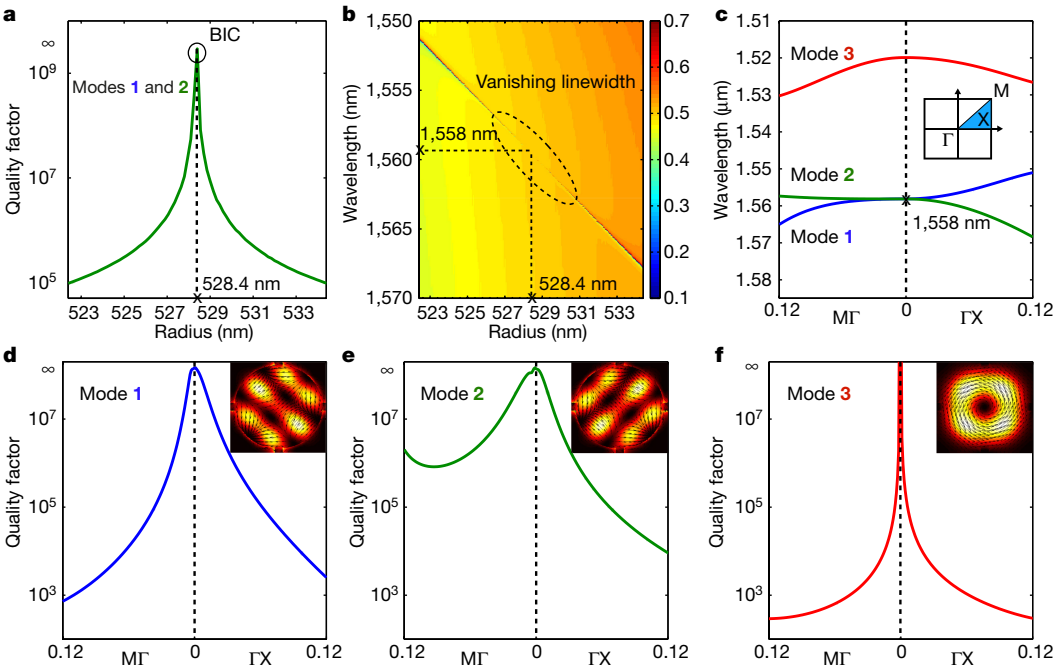

Figure 2 | Design and complex dispersion relation of the BIC cavity. a, Quality factor of high-Q modes at the Γ point around the telecommunication wavelength for different nanoresonator radii. The quality factors of modes 1 and 2, which are doubly degenerate at the Γ point, are strongly dependent on the radius R. For $R = R_{opt}$ at 528.4 nm, this quality factor approaches infinity to form a resonance-trapped BIC. For radii around R_{opt} the quality factor remains very high. **b**, Transmission spectrum at normal incidence showing the vanishing linewidth of modes 1 and 2 when the radius approaches R_{opt}. The wavelength of the modes is a function of the radius and it continuously varies between the smallest radius ($R = 522$ nm) and the largest radius ($R = 534$ nm). **c**, Dispersion relation around 1.55 μm for high-Q modes (1, 2 and 3) in both MΓ and ΓX directions as a function of $k(a/2\pi)$. The inset shows the first Brillouin zone of the square lattice and irreducible contour for cylindrical nanoresonators (shaded area). The contour connects high-symmetry points Γ, X, and M. **d–f**, Quality factor of high-Q modes in both the MΓ and the ΓX direction for mode 1 (**d**), mode 2 (**e**), and mode 3 (**f**). Insets represent the normalized electric field on the surface of a unit cell. Modes 1 and 2 are identical under 90-degree rotation. Mode 3 is a symmetry-protected mode and is thus not affected by geometrical changes that preserve symmetry, such as the change of radius. The quality factor of mode 3, however, drops rapidly away from the high-symmetry point Γ. It drops more rapidly compared to the quality factor of modes 1 and 2. The sharper drop of the quality factor of mode 3 away from Γ implies that the integrated quality factor of this mode will be smaller than those of modes 1 and 2 in the case of finite-sized samples.

© 2017 Macmillan Publishers Limited, part of Springer Nature. All rights reserved.

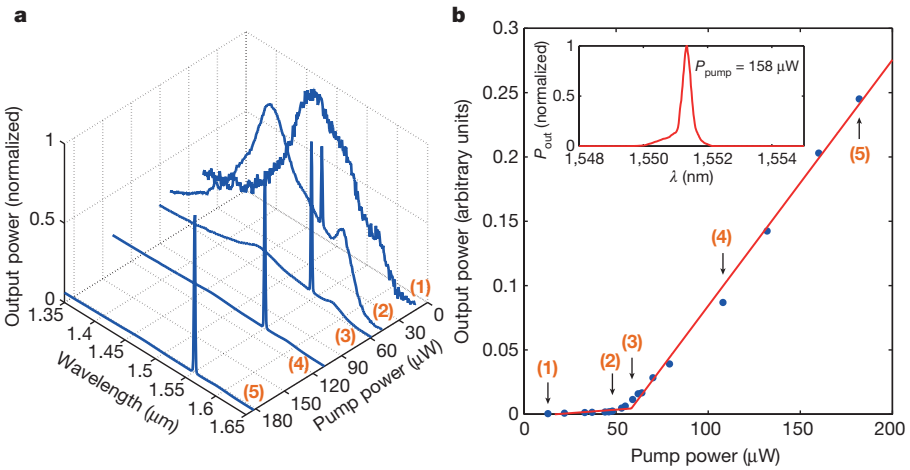

Figure 3 | Experimental characterization of the BIC laser. a, Evolution of the normalized output power as a function of wavelength and pump power for a 16-by-16 array with a nanoresonator radius of 525 nm. We observe the transition from a broad spontaneous emission to a single lasing peak at 1,551.4 nm. **b**, Output power as a function of the average pump power (light–light curve) around the lasing wavelength. We observe the onset of lasing at a threshold power of 56 μW. The red lines are linear fits to the data, indicating the regions of spontaneous and stimulated emission. The blue dots correspond to measurements and numbers (1) to (5) denote the spectra plotted in **a**. Here the standard error in arbitrary units is less than 0.01. The inset shows the lasing spectrum at a pump power of 158 μW with a measured linewidth of about 0.33 nm (detection-limited).

degenerate away from the Γ point (as seen in Fig. 2c), do not drop as sharply as that of mode 3. Modes 1 and 2 are thus much less sensitive to symmetry-breaking perturbations. Additionally, the resonance-trapped BIC is robust because a variation in radius only induces its displacement in *k*-space (reciprocal space, where *k* is the wavevector), whereas a symmetry-breaking perturbation destroys the symmetry-protected mode[13]. This is of utmost importance in device design as fabrication tolerances will have less impact on resonance-trapped BICs than on modes that rely on symmetry protection. Moreover, designing a mode with a high quality factor in a large region of *k*-space is of practical importance because fabricated devices, which are never spatially infinite, always sample the dispersion relation in a finite neighbourhood in *k*-space[28]. Therefore, for a given quality factor, we can achieve a much smaller device footprint with a resonance-trapped BIC mode than with symmetry-protected modes.

To experimentally demonstrate lasing from our BIC cavity, we optically pump the membrane at room temperature with a pulsed laser ($\lambda = 1{,}064$ nm, $T = 12$ ns pulse at a repetition rate $f = 300$ kHz) and record the spectral emission (see section F of Supplementary

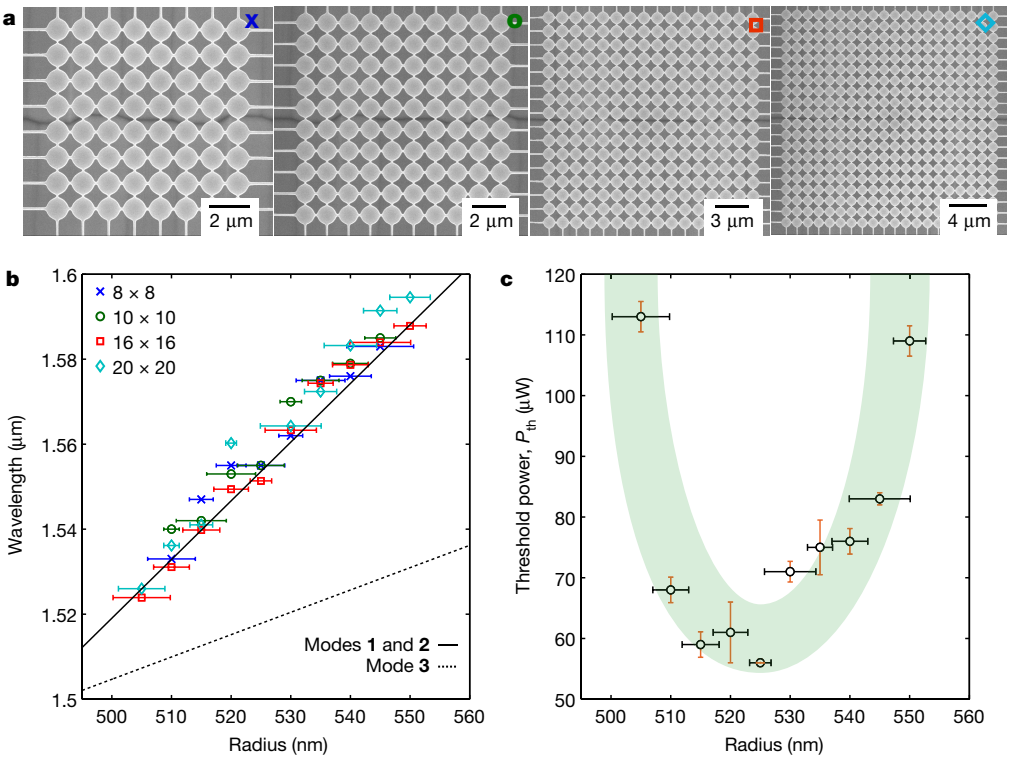

Figure 4 | Scaling of the BIC lasers. a, Electron micrographs of fabricated BIC lasers of size 8-by-8, 10-by-10, 16-by-16, and 20-by-20. **b**, Lasing wavelength as a function of nanoresonator radius, from 500 nm to 550 nm, with array sizes of 8-by-8 (cross), 10-by-10 (circle), 16-by-16 (square), and 20-by-20 (diamond). Each point corresponds to a device with a specific radius, bridge width and array size. Error bars indicate the standard deviation of radii measured from fabricated devices. The lines represent the theoretical resonant wavelength of modes 1 and 2 (solid line) and 3 (dashed line) for different radii of nanoresonators, for the infinite array. The good agreement between the experimental lasing wavelengths and the theoretical resonant wavelengths of the resonance-trapped BIC mode (modes 1 and 2) confirms that lasing action is indeed from the BIC mode. **c**, Additionally, measured threshold power as a function of radii for the lasers clearly shows a minimum (56 μW) close to R_{opt} (about 525 nm) reflecting the maximum quality factor around the BIC singularity and offers further proof of lasing action from the BIC mode (modes 1 and 2). The inverse relationship between quality factor and threshold is evident (see section G of Supplementary Information). Mode 3 has no variation in quality factor with radii. The vertical error bars are the standard error in the threshold power estimated over multiple measurements (varying pump power) repeated more than three times whereas the horizontal error bars represent the standard deviation of measured radii. The green shaded area is a guide to the eye.

© 2017 Macmillan Publishers Limited, part of Springer Nature. All rights reserved.

Information). Figure 3a shows the evolution of the output power as a function of both the pump power and the wavelength. At low pump power, we observe a spectrally broad photoluminescence spectrum, while at high pump power, we observe a drastic overall suppression of the photoluminescence in favour of one extremely narrow peak, that is, lasing. As depicted in Fig. 3a, three modes show amplification at first ($P_{pump} \approx 48\,\mu W$) but, ultimately, only one remains. Lasing action occurs at a wavelength of 1,551.4 nm with a detection-limited linewidth of about 0.33 nm (see inset of Fig. 3b). Figure 3b shows the evolution of the output power as a function of the pump power around this lasing wavelength. We observe a clear threshold behaviour with a threshold power of 56 μW or a density of 140 mW mm^{-2}.

To further demonstrate the robustness and scalability[29] of our BIC laser, we fabricated several devices (36 devices) with a range of radii and array sizes as seen in Fig. 4a. Figure 4b shows the measured lasing wavelength of devices of different array size (8-by-8, 10-by-10, 16-by-16 and 20-by-20), and different radii of nanoresonators. The solid and dashed lines represent, respectively, the theoretical resonant wavelength of modes 1 and 2 and mode 3 for different radii of nanoresonators in the infinite array. We observe a very good agreement between the experimental lasing wavelengths and the theoretical resonant wavelengths of the resonance-trapped BIC mode (modes 1 and 2). This agreement confirms that lasing action is indeed from the BIC mode over the entire range of radii. Moreover, the persistence of lasing for all array sizes down to as few as 8-by-8 nanoresonators shows the scalability of our BIC laser, thanks to the large quality factor of the resonance-trapped BIC mode in a wide region of k-space. Further evidence of lasing from the BIC mode can directly be observed in the measured threshold power of the lasers. The threshold power has a clear minimum close to R_{opt} (about 525 nm), reflecting a maximum quality factor at the BIC singularity as seen in Fig. 4c. Also see section G of Supplementary Information for a discussion on the influence of quality factor for a finite cavity on the lasing threshold. Additional characterization such as far-field profiles and polarization measurements of these lasing devices are provided in section H of Supplementary Information.

We have thus reported a BIC laser from a cavity mode that can, surprisingly, have arbitrarily high quality factors despite being embedded in the continuum of radiation modes. This cavity, made of an array of suspended cylindrical nanoresonators, shows persistent single-mode lasing for various radii and array sizes. The lasing wavelength follows the theoretical prediction of the BIC mode and the inverse relationship between quality factor and lasing threshold is experimentally demonstrated. These results demonstrate the robustness and scalability of the system. The ability to confine light within the radiation continuum opens up the study of the intriguing topological physics of BICs and the realization of non-standard photonic devices, sensors and sources.

Online Content Methods, along with any additional Extended Data display items and Source Data, are available in the online version of the paper; references unique to these sections appear only in the online paper.

Data Availability The data that support the findings of this study are available from the corresponding author upon reasonable request.

Received 8 July; accepted 8 November 2016.

1. von Neumann, J. & Wigner, E. On some peculiar discrete eigenvalues. *Phys. Z.* **30,** 467 (1929).
2. Herrick, D. R. Construction of bound states in the continuum for epitaxial heterostructure superlattices. *Physica B* **85,** 44–50 (1976).
3. Stillinger, F. H. Potentials supporting positive-energy eigenstates and their application to semiconductor heterostructures. *Physica B* **85,** 270–276 (1976).
4. Friedrich, H. & Wintgen, D. Interfering resonances and bound states in the continuum. *Phys. Rev. A* **32,** 3231–3242 (1985).
5. Hsu, C. W., Zhen, B., Stone, A. D., Joannopoulos, J. D. & Soljačić, M. Bound states in the continuum. *Nat. Rev. Mater.* **1,** 16048 (2016).
6. Linton, C. M. & McIver, P. Embedded trapped modes in water waves and acoustics. *Wave Motion* **45,** 16–29 (2007).
7. Lepetit, T. & Kanté, B. Controlling multipolar radiation with symmetries for electromagnetic bound states in the continuum. *Phys. Rev. B* **90,** 241103(R) (2014).
8. Marinica, D. C. *et al.* Bound states in the continuum in photonics. *Phys. Rev. Lett.* **100,** 183902 (2008).
9. Bulgakov, E. N. & Sadreev, A. F. Bound states in the continuum in photonic waveguides inspired by defects. *Phys. Rev. B* **78,** 075105 (2008).
10. Dreisow, F. *et al.* Adiabatic transfer of light via a continuum in optical waveguides. *Opt. Lett.* **34,** 2405–2407 (2009).
11. Plotnik, Y. *et al.* Experimental observation of optical bound states in the continuum. *Phys. Rev. Lett.* **107,** 183901 (2011).
12. Weimann, S. *et al.* Compact surface Fano states embedded in the continuum of waveguide arrays. *Phys. Rev. Lett.* **111,** 240403 (2013).
13. Hsu, C. W. *et al.* Observation of trapped light within the radiation continuum. *Nature* **499,** 188–191 (2013).
14. Monticone, F. & Alù, A. Embedded photonic eigenvalues in 3D nanostructures. *Phys. Rev. Lett.* **112,** 213903 (2014).
15. Molina, M. I., Miroshnichenko, A. E. & Kivshar, Y. S. Surface bound states in the continuum. *Phys. Rev. Lett.* **108,** 070401 (2012).
16. Zhang, M. & Zhang, X. Ultrasensitive optical absorption in graphene based on bound states in the continuum. *Sci. Rep.* **5,** 8266 (2015).
17. Zhen, B., Hsu, C. W., Lu, L., Stone, A. D. & Soljačić, M. Topological nature of optical bound states in the continuum. *Phys. Rev. Lett.* **113,** 257401 (2014).
18. Miyai, E. *et al.* Photonics: Lasers producing tailored beams. *Nature* **441,** 946 (2006).
19. Sadreev, A. F., Bulgakov, E. N. & Rotter, I. Bound states in the continuum in open quantum billiards with a variable shape. *Phys. Rev. B* **73,** 235342 (2006).
20. Wiersig, J. Formation of long-lived, scarlike modes near avoided resonance crossings in optical microcavities. *Phys. Rev. Lett.* **97,** 253901 (2006).
21. Persson, E., Rotter, I., Stöckmann, H.-J. & Barth, M. Observation of resonance trapping in an open microwave cavity. *Phys. Rev. Lett.* **85,** 2478–2481 (2000).
22. Sakoda, K. *Optical Properties of Photonic Crystals* Chs 3, 8 (Springer, 2005).
23. Fan, S. & Joannopoulos, J. D. Analysis of guided resonances in photonic crystal slabs. *Phys. Rev. B* **65,** 235112 (2002).
24. Yang, Y., Peng, C., Liang, Y., Li, Z. & Noda, S. Analytical perspective for bound states in the continuum in photonic crystal slabs. *Phys. Rev. Lett.* **113,** 037401 (2014).
25. Kogelnik, H. & Shank, C. V. Stimulated emission in a periodic structure. *Appl. Phys. Lett.* **18,** 152–154 (1971).
26. Meier, M. *et al.* Laser action from two-dimensional distributed feedback in photonic crystals. *Appl. Phys. Lett.* **74,** 7–9 (1999).
27. Imada, M. *et al.* Coherent two-dimensional lasing action in surface-emitting laser with triangular lattice photonic crystal structure. *Appl. Phys. Lett.* **75,** 316–318 (1999).
28. Xu, T., Yang, S., Nair, S. V. & Ruda, H. E. Confined modes in finite-size photonic crystals. *Phys. Rev. B* **72,** 045126 (2005).
29. Koenderink, A. F., Alù, A. & Polman, A. Nanophotonics: Shrinking light-based technologies. *Science* **348,** 516–521 (2015).

Supplementary Information is available in the online version of the paper.

Acknowledgements This research was supported by the National Science Foundation Career Award (ECCS-1554021), the Office of Naval Research Multi-University Research Initiative (N00014-13-1-0678), and the startup funds provided to B.K. by the University of California San Diego. The work was performed in part at the San Diego Nanotechnology Infrastructure, a member of the National Nanotechnology Coordinated Infrastructure, which is supported by the National Science Foundation (ECCS-1542148). We thank M. Montero for technical assistance regarding the fabrication.

Author Contributions B.K. conceived the project. A.K. and Q.G. fabricated the samples and performed the measurements. T.L. and B.B. performed the theoretical calculations. B.K., T.L., and Y.F. guided the theoretical and experimental investigations. All authors contributed to discussions and manuscript writing.

Author Information Reprints and permissions information is available at www.nature.com/reprints. The authors declare no competing financial interests. Readers are welcome to comment on the online version of the paper. Correspondence and requests for materials should be addressed to B.K. (bkante@ucsd.edu).

© 2017 Macmillan Publishers Limited, part of Springer Nature. All rights reserved.